Weierstraß-Institut
für Angewandte Analysis und Stochastik
Leibniz-Institut im Forschungsverbund Berlin e. V.

Preprint ISSN 2198-5855

Thin-film models for viscoelastic liquid bi-layers

Sebastian Jachalski[1], Andreas Münch[2], Barbara Wagner[1,3]

submitted: December 7, 2015

[1] Weierstrass Institute
Mohrenstr. 39
10117 Berlin
Germany
E-Mail: sebastian.jachalski@wias-berlin.de
barbara.wagner@wias-berlin.de

[2] Mathematical Institute
University of Oxford
24-29 St. Giles'
Oxford OX1 3LB, UK
E-Mail: muench@maths.ox.ac.uk

[3] Institute of Mathematics
Technische Universität Berlin
Straße des 17. Juni 136
10623 Berlin
Germany

No. 2187
Berlin 2015

Key words and phrases. fluid dynamics; viscoelasticty; thin-film models; two-phase flow; asymptotic methods; numerical solution.

Part of this work was supported by DFG through the SPP 1506 *transport processes at fluidic interfaces*.

Edited by
Weierstraß-Institut für Angewandte Analysis und Stochastik (WIAS)
Leibniz-Institut im Forschungsverbund Berlin e. V.
Mohrenstraße 39
10117 Berlin
Germany

Fax: +49 30 20372-303
E-Mail: preprint@wias-berlin.de
World Wide Web: http://www.wias-berlin.de/

Abstract

In this work we consider a two-layer system of viscoelastic liquids of corotational Jeffreys' type dewetting from a Newtonian liquid substrates. We derive conditions that allow for the first time the asymptotically consistent reduction of the free boundary problem for the two-layer system to a system of coupled thin-film equations that incorporate the full nonlinear viscoelastic rheology. We show that these conditions are controlled by the order of magnitude of the viscosity ratio of the liquid layers and their thickness ratio. For pure Newtonian flow, these conditions lead to a thin-film model that couples a layer with a parabolic flow field to a layer described by elongational flow. For this system we establish asymptotic regimes that relate the viscosity ratio to a corresponding apparent slip. We then use numerical simulations to discuss the characteristic morphological and dynamical properties of viscoelastic films of corotational Jeffreys' type dewetting from a solid as well as liquid substrate.

1 Introduction

Liquid two-layer systems frequently combine layers of different rheological and interfacial properties to be exploited in nature and in various technological applications, for example for process engineering organic photovoltaics devices or similar processes used in the semi-conductor industry [4, 14, 20, 25, 27]. For many of these applications the dimensions, in particular the thickness, of the layers are in the micro- to nanometer range so that rupture and subsequent liquid dewetting become important problems that need to be understood.

The mathematical boundary value problem of the two-layer system governing these processes often involve layers of viscoelastic polymers besides Newtonian liquids, together with free and interfacial boundaries. For two-layer thin films of Newtonian liquids it has been shown in the past that the asymptotic reduction of the governing equations to a system of thin-film models can be achieved via a lubrication type approximation by making use of the scale separation between horizontal and vertical dimensions [1, 10, 17, 23, 28, 35]. The availability of such dimension-reduced models bears great advantages for the analysis and numerical simulation of the underlying free boundary problem and becomes even more important if the focus of interest lies in the formation and design of three-dimensional patterns.

For two-layer systems that incorporate nonlinear viscoelastic rheologies, such as the corotational Jeffreys' model or the better known Oldroyd-B model, similar derivations of thin-film models have not been investigated so far. In fact, for the simpler situation of the flow of a single liquid layer on a solid substrate an asymptotically consistent derivation of closed form lubrication approximations that incorporate nonlinear viscoelastic rheologies is in general not possible

[6, 30, 43]. However, as has been shown in [32], when it is assumed that friction at the boundary with the substrate is reduced by allowing the liquid film to slip along the substrate, then the nonlinear corotational Jeffreys model can be fully incorporated into a thin-flim approximation. Specifically, it is shown there that an asymptotically consistent derivation of the thin-film model requires the slip-length to be of order of magnitude much larger than the thickness of the dewetting layer.

In this study we show that for the two-layer system of a nonlinear viscoelastic liquid film dewetting from a liquid substrate an asymptotically consistent thin-film approximation can be obtained if the viscosity of the liquid substrate is much smaller than the one of the dewetting layer. We argue that this regime gives rise to a plug flow in the dewetting layer, so that the normal stresses remain asymptotically consistent with the thin film approximation. In fact, if both layers are Newtonian the analogous conclusion can be drawn, that is, a thin-film equation for plug-flow including extensional stresses is obtained for the dewetting layer.

The connection between low viscosity of the liquid substrate and plug flow in the dewetting layer has already been made by Brochard et al. [8] and Joanny et al. [24] but without taking viscoelastic effects into account. On the other hand, for the single layer situation with slip at the solid substrate, the importance of extensional stresses in plug flow regimes has been explored theoretically and experimentally only recently, for example in [2, 15, 33].

In this work after the formulation of the free boundary problem in Section 2, we combine both ideas to derive a class of thin film models which incorporate also extensional stresses in the thin-film approximation in Section 3. We show transitions in flow regimes by varying the order of magnitude of the viscosity ratios of the liquid layers as well as their thicknesses. We show that these regimes produce characteristic dewetting profiles for the dewetting layer as well as for the interface with the underlying liquid substrate.

For the special case of an undeformable interface with the liquid substrate and for increasing surface tension with the substrate, we show in Section 4 that the transitions in flow regimes and the corresponding surface profiles of the dewetting layer can be brought in one-to-one correspondence with the previously discussed transitions for moderate to large slip boundary conditions, that has been investigated in the past [33]. Finally, in Section 5 we use these results on the flow regimes and profile transitions to study the specific signatures when nonlinear viscoelastic effects of the corotational Jeffreys type and extensional stresses are incorporated in the thin-film approximation to leading order.

2 Formulation of the free-boundary problem

Constitutive laws that model the viscoelastic properties of polymer melts such as Polystyrene (PS) or Polydimethylsiloxane (PDMS) often use some form of a generalized Maxwell or Jeffreys model or alternatively, Oldroyd's model, see Hassager et al. [36] for detailed derivations and discussions. In the context of thin-film flows of polymer melts, various viscoelastic models have been discussed in the past, [6, 7, 21, 26, 37, 41] to explain the morphology and other characteristics of dewetting polymer films from a solid substrate. For the study of two-layer liquid systems considered here, we use the corotational Jeffreys model in the governing equations

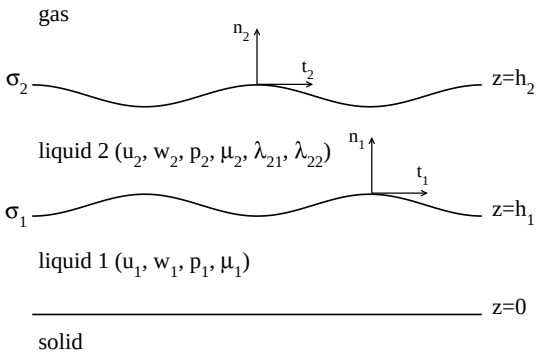

Figure 1: Sketch of the bi-layer system.

for the upper layer to reflect advective and corotational nonlinearities, while we let the substrate layer obey Newtonian flow behaviour.

The set-up of the liquid-liquid system is shown in the sketch in fig. 1. First, we define two domains which are occupied by the liquids by

$$\Omega_1 := \{(x,z,t)|\, 0 \leq z \leq h_1(x,t)\}, \qquad \Omega_2 := \{(x,z,t)|\, h_1(x,t) \leq z \leq h_2(x,t)\}, \quad (1)$$

where $h_1(x,t)$ denotes the interfacal free boundary between the lower and upper liquid layer, $h_2(x,t)$ is the free boundary to the ambient gas. From this point on we denote quantities which are related to the lower liquid by index 1. Analogously we use index 2 for quantities which are related to the upper layer.

The governing equations for the evolution of the liquid layers within the domains Ω_1 and Ω_2 are given by the continuity equation for both layers and the Cauchy momentum equations

$$0 = \partial_x u_i + \partial_z w_i, \quad (2a)$$

$$\rho_i \frac{d}{dt} u_i = -\partial_x p_i + \partial_x \tau_{i,11} + \partial_z \tau_{i,12}, \quad (2b)$$

$$\rho_i \frac{d}{dt} w_i = -\partial_z p_i + \partial_x \tau_{i,12} + \partial_z \tau_{i,22}, \quad (2c)$$

where u_i and w_i denote the velocities in the horizontal and vertical direction, respectively, ρ_i are the densities of the liquid layers and p_i denote the hydrostatic pressures.

In the upper viscoelastic layer we assume that the symmetric stress tensor τ_2 obeys the corotational Jeffreys model with the constutitve equation

$$\tau_2 + \lambda_{21} \frac{D}{Dt} \tau_2 = \mu_2 \left(\dot{\gamma}_2 + \lambda_{22} \frac{D}{Dt} \dot{\gamma}_2 \right), \quad (3)$$

and where the Jaumann derivative D/Dt is defined by

$$\frac{D\Lambda}{Dt} = \frac{d\Lambda}{dt} + \frac{1}{2} \left(\omega_2 \Lambda - \Lambda \omega_2 \right), \quad (4)$$

for an arbitrary tensor field Λ. The strain rate $\dot{\gamma}_2$ is given by

$$\dot{\gamma}_2 = \begin{pmatrix} 2\partial_x u_2 & \partial_z u_2 + \partial_x w_2 \\ \partial_z u_2 + \partial_x w_2 & 2\partial_z w_2 \end{pmatrix}, \tag{5}$$

and the vorticity tensor is

$$\omega_2 = \begin{pmatrix} 0 & \partial_x w_2 - \partial_z u_2 \\ \partial_z u_2 - \partial_x w_2 & 0 \end{pmatrix}. \tag{6}$$

Since the lower layer is assumed to behave as a Newtonian fluid, the stress tensor τ_1 is proportional to the strain rate $\dot{\gamma}_1$.

$$\tau_1 = \mu_1 \begin{pmatrix} 2\partial_x u_1 & \partial_z u_1 + \partial_x w_1 \\ \partial_z u_1 + \partial_x w_1 & 2\partial_z w_1 \end{pmatrix}. \tag{7}$$

In this work we assume the viscosities μ_1 and μ_2 as well as the relaxation parameters λ_{21} and λ_{22} to be constant material parameters. The relaxation parameter λ_{21} typically denotes a measure of the time required for the stress to relax to some limiting value, whereas λ_{22} is a measure of the retardation to return to the equilibrium state, see for example [36].

The geometry of the problem yield three boundaries, one at the solid substrate, and two free boundaries at the liquid-liquid interface and one at the free boundary with the ambient gas or air. At the solid boundary, which is here at $z = 0$ we assume no-slip and impermeability conditions.

$$u_1 = 0, \qquad w_1 = 0. \tag{8a}$$

At the liquid-liquid interface $z = h_1$ we obtain the kinematic condition

$$\partial_t h_1 = w_1 - \partial_x h_1 u_1, \tag{8b}$$

Also we assume that the tangential and normal stress force balances

$$(\tau_{1,12} - \tau_{2,12})\left(1 - (\partial_x h_1)^2\right) + \big((\tau_{1,22} - \tau_{1,11}) - (\tau_{2,22} - \tau_{2,11})\big)\partial_x h_1 = 0, \tag{8c}$$

and

$$\begin{aligned} &- p_1 + p_2 - \phi'(h) + \frac{(\tau_{1,11} - \tau_{2,11})(\partial_x h_1)^2 - 2(\tau_{1,12} - \tau_{2,12})\partial_x h_1 + (\tau_{1,22} - \tau_{2,22})}{1 + (\partial_x h_1)^2} \\ &= \sigma_1 \frac{\partial_{xx} h_1}{\left(1 + (\partial_x h_1)^2\right)^{3/2}}, \end{aligned} \tag{8d}$$

are satisfied, respectively, where where $\phi'(h)$ is a function of the thickness of the top layer $h := h_2 - h_1$ and denotes the disjoining pressure arising from the intermolecular van der Waals forces that drive the rupture and subsequent dewetting of the upper layer, combined with a stabilizing contribution at very small thicknesses arising from Born repulsion forces. A typical choice for the intermolecular potential $\phi(h)$ is

$$\phi(h) = \frac{8}{3}\phi_* \left[\frac{1}{8}\left(\frac{h_*}{h}\right)^8 - \frac{1}{2}\left(\frac{h_*}{h}\right)^2\right], \tag{8e}$$

where here the choice of constants is such that $\phi_* < 0$ is the minimum of the potential at $h = h_*$, which is the thickness that remains after the film has dewetted, see for example [23].

We assume no-slip and impermeability at $z = h_1$ which yield the corresponding conditions

$$(u_2 - u_1) + (w_2 - w_1)\partial_x h_1 = 0, \qquad -(u_2 - u_1)\partial_x h_1 + (w_2 - w_1) = 0. \tag{8f}$$

Similarly, we obtain for the boundary conditions at the free boundary $z = h_2$ the kinematic condition,

$$\partial_t h_2 = w_2 - \partial_x h_2 u_2, \tag{8g}$$

and the tangential and normal stress force balances

$$\tau_{2,12}\left(1 - (\partial_x h_2)^2\right) + (\tau_{2,22} - \tau_{2,11})\,\partial_x h_2 = 0, \tag{8h}$$

and

$$-p_2 + \phi'(h) + \frac{\tau_{2,11}(\partial_x h_2)^2 - 2\tau_{2,12}\partial_x h_2 + \tau_{2,22}}{1 + (\partial_x h_2)^2} = \sigma_2 \frac{\partial_{xx} h_2}{\left(1 + (\partial_x h_2)^2\right)^{3/2}}. \tag{8i}$$

3 Thin-film model for the viscoelastic bi-layer

3.1 Scaled problem

For the nondimensional problem we introduce the following dimensionless quantities

$$x = Lx^*, \qquad (z, h_i) = H(z^*, h_i^*), \qquad (t, \lambda_{21}, \lambda_{22}) = T(t^*, \lambda_{21}^*), \tag{9a}$$

$$(u_1, u_2) = U(u_1^*, u_2^*), \qquad (w_1, w_2) = W(w_1^*, w_2^*), \qquad (p_i, \phi') = P(p_i^*, \phi'^*), \tag{9b}$$

where L and H denote the characteristic length scales and U, W the characteristic velocity scales in the vertical and horizontal direction, respectively. For the stress tensors we set

$$\begin{pmatrix} \tau_{i,11} & \tau_{i,12} \\ \tau_{i,21} & \tau_{i,22} \end{pmatrix} = \frac{\mu_i}{T} \begin{pmatrix} \tau_{i,11}^* & \frac{L}{H}\tau_{i,12}^* \\ \frac{L}{H}\tau_{i,21}^* & \tau_{i,22}^* \end{pmatrix}. \tag{10}$$

For the system of thin liquid layers the characteristic length scales of the evolving patterns in the horizontal direction are much larger than the typical scale of the heights h_i. We thus introduce the small parameter

$$\varepsilon := \frac{H}{L} = \sqrt{\frac{8}{3}\frac{\phi*}{\sigma_2}} \ll 1 \tag{11}$$

which is fixed by the pressure scale from the intermolecular potential, i.e. $P = 8\phi * /3H$. In view of the kinematic conditions determine the timescale via

$$T = \frac{L}{U}, \tag{12}$$

Balancing the terms in the stress force conditions yields the relations

$$P = \frac{\sigma_2 H}{L^2} \qquad \text{and} \quad \frac{\mu_2 U}{\sigma_2} = \varepsilon. \tag{13}$$

In [32] it has been argued that in order to incorporates the full corotational Jeffreys constitutive law the boundary condition with the substrate needs to allow for large apparent slip on order of magnitude $O(\varepsilon^{-2})$. For liquid two-layer systems we argue here, that an analogous condition that allows the derivation of a thin-film model and also captures the nonlinear features of the corotational Jeffreys model, requires the ratio of the viscosities of the two layers to be of order of magnitude $O(\varepsilon^{-2})$.

In this case we assume

$$\mu := \frac{\mu_1}{\mu_2}\varepsilon^{-2} = O(1), \tag{14}$$

keeping the ratio of the surface tensions $\sigma := \sigma_1/\sigma_2 = O(1)$.

Assuming the relationships in 14 we obtain for the non-dimensional equations in the bulk

$$\partial_x u_1 + \partial_z w_1 = 0, \qquad \partial_x u_2 + \partial_z w_2 = 0, \tag{15a}$$

$$0 = -\varepsilon^2 \partial_x p_1 + \varepsilon^4 \mu \partial_{xx} u_1 + \varepsilon^2 \mu \partial_{zz} u_1, \tag{15b}$$
$$0 = -\partial_z p_1 + \varepsilon^2 \mu \partial_{xx} w_1 + \varepsilon^2 \mu \partial_{zz} w_1, \tag{15c}$$

$$0 = -\varepsilon^2 \partial_x p_2 + \varepsilon^2 \partial_x \tau_{2,11} + \partial_z \tau_{2,12}, \tag{15d}$$
$$0 = -\partial_z p_2 + \partial_x \tau_{2,12} + \partial_z \tau_{2,22}, \tag{15e}$$

where the stress tensor of the upper liquids fulfil

$$\begin{aligned} &\left(1 + \lambda_{21}\frac{d}{dt}\right)\tau_{2,11} - \lambda_{21}\left(\frac{1}{\varepsilon^2}\partial_z u_2 - \partial_x w_2\right)\tau_{2,12} \\ &= 2\left(1 + \lambda_{22}\frac{d}{dt}\right)\partial_x u_2 - \lambda_{22}\left(\left(\frac{1}{\varepsilon}\partial_z u_2\right)^2 - (\varepsilon \partial_x w_2)^2\right), \end{aligned} \tag{16a}$$

$$\begin{aligned} &\left(1 + \lambda_{21}\frac{d}{dt}\right)\tau_{2,22} + \lambda_{21}\left(\frac{1}{\varepsilon^2}\partial_z u_2 - \partial_x w_2\right)\tau_{2,12} \\ &= 2\left(1 + \lambda_{22}\frac{d}{dt}\right)\partial_z w_2 + \lambda_{22}\left(\left(\frac{1}{\varepsilon}\partial_z u_2\right)^2 - (\varepsilon \partial_x w_2)^2\right), \end{aligned} \tag{16b}$$

$$\begin{aligned} &\left(1 + \lambda_{21}\frac{d}{dt}\right)\tau_{2,12} + \frac{\lambda_{21}}{2}\left(\partial_z u_2 - \varepsilon^2 \partial_x w_2\right)\left(\tau_{2,11} - \tau_{2,22}\right) \\ &= \left(1 + \lambda_{22}\frac{d}{dt}\right)\left(\partial_z u_2 + \varepsilon^2 \partial_x w_2\right) + 2\lambda_{22}\left(\partial_z u_2 - \varepsilon^2 \partial_x w_2\right)\partial_x u_2. \end{aligned} \tag{16c}$$

The boundary conditions at $z = 0$ are

$$u_1 = 0, \qquad w_1 = 0. \tag{17}$$

The equations at $z = h_1$ become

$$\partial_t h_1 = w_1 - \partial_x h_1 u_1. \tag{18}$$

$$\left(\varepsilon^2\mu(\partial_z u_1 + \varepsilon^2\partial_x w_1) - \tau_{2,12}\right)\left(1 - (\varepsilon\partial_x h_1)^2\right) \tag{19}$$

$$+\varepsilon^2\big(2\varepsilon^2\mu(\partial_z w_1 - \partial_x u_1) - (\tau_{2,22} - \tau_{2,11})\big)\partial_x h_1 = 0, \tag{20}$$

$$\begin{aligned} &- p_1 + p_2 - \phi'(h) + \frac{\left(2\varepsilon^2\mu\partial_x u_1 - \tau_{2,11}\right)\left(\varepsilon\partial_x h_1\right)^2}{1 + \left(\varepsilon\partial_x h_1\right)^2} \\ &- \frac{2(\varepsilon^2\mu(\partial_z u_1 + \varepsilon^2\partial_x w_1) - \tau_{2,12})\partial_x h_1 - (2\varepsilon^2\mu\partial_z w_1 - \tau_{2,22})}{1 + \left(\varepsilon\partial_x h_1\right)^2} \\ &= \frac{\sigma\partial_{xx} h_1}{\left(1 + \left(\varepsilon\partial_x h_1\right)^2\right)^{3/2}}, \end{aligned} \tag{21}$$

and

$$(u_2 - u_1) + \varepsilon^2(w_2 - w_1)\partial_x h_1 = 0, \qquad -(u_2 - u_1)\partial_x h_1 + (w_2 - w_1) = 0. \tag{22}$$

At $z = h_2$ we obtain

$$\partial_t h_2 = w_2 - \partial_x h_2 u_2. \tag{23}$$

$$\tau_{2,12}\left(1 - \left(\varepsilon\partial_x h_2\right)^2\right) + \varepsilon^2\left(\tau_{2,22} - \tau_{2,11}\right)\partial_x h_2 = 0, \tag{24}$$

and

$$- p_2 + \phi'(h) + \frac{\tau_{2,11}\left(\varepsilon\partial_x h_2\right)^2 - 2\tau_{2,12}\partial_x h_2 + \tau_{2,22}}{1 + \left(\varepsilon\partial_x h_2\right)^2} = \frac{\partial_{xx} h_2}{\left(1 + \left(\varepsilon\partial_x h_2\right)^2\right)^{3/2}}. \tag{25}$$

3.2 Thin-film model

We will now show that to leading order in ε the free boundary problem can be integrated and reduced to a system of coupled partial differential equations for the height h, h_1, u_2 and S. To leading order the equations in the bulk of the lower liquid and in the upper liquid are

$$\partial_x u_1 + \partial_z w_1 = 0, \qquad 0 = -\partial_x p_1 + \mu\partial_{zz} u_1, \qquad 0 = -\partial_z p_1 \tag{26a}$$

and

$$\partial_x u_2 + \partial_z w_2 = 0, \qquad 0 = \partial_z \tau_{2,12}, \qquad 0 = -\partial_z p_2 + \partial_x \tau_{2,12} + \partial_z \tau_{2,22}, \tag{26b}$$

where

$$\lambda_{21}\partial_z u_2 \tau_{2,12} = \lambda_{22}\left(\partial_z u_2\right)^2 \tag{26c}$$

and

$$\left(1+\lambda_{21}\frac{d}{dt}\right)\tau_{2,12} + \frac{\lambda_{21}}{2}\partial_z u_2(\tau_{2,11}-\tau_{2,22}) = \left(1+\lambda_{22}\frac{d}{dt}\right)\partial_z u_2 + 2\lambda_{22}\partial_z u_2 \partial_x u_2. \tag{26d}$$

The boundary conditions are

$$u_1 = 0, \qquad w_1 = 0 \tag{26e}$$

at $z = 0$,

$$\partial_t h_1 = w_1 - \partial_x h_1 u_1, \tag{26f}$$

$$\tau_{2,12} = 0, \qquad -p_1 + p_2 - \phi'(h) - \tau_{2,22} = \sigma\partial_{xx} h_1, \tag{26g}$$

$$u_2 - u_1 = 0, \qquad -(u_2-u_1)\partial_x h_1 + (w_2 - w_1) = 0, \tag{26h}$$

at $z = h_1$ and

$$\partial_t h_2 = w_2 - \partial_x h_2 u_2, \tag{26i}$$

$$\tau_{2,12} = 0, \qquad -p_2 + \phi'(h) + \tau_{2,22} = \partial_{xx} h_2 \tag{26j}$$

at $z = h_2$.

In order to obtain a closed set of equation we also need to account for the some relations for the stress tensor from the next order problem, where we have expanded the variables u_i, w_i, p_i, $\tau_{i,jk}$ with $i, j, k \in 1, 2$ as $u_i = u_i^{(0)} + \varepsilon^2\, u_i^{(1)} + O(\varepsilon^4)$ and likewise with the other variables. For ease of notation we then dropped the $^{(0)}$ from the leading order variables. The relations we need are,

$$0 = -\partial_x p_2 + \partial_x \tau_{2,11} + \partial_z \tau_{2,12}^{(1)}, \tag{27a}$$

$$\left(1+\lambda_{21}\frac{d}{dt}\right)\tau_{2,11} = 2\left(1+\lambda_{22}\frac{d}{dt}\right)\partial_x u_2, \tag{27b}$$

$$\left(1+\lambda_{21}\frac{d}{dt}\right)\tau_{2,22} = 2\left(1+\lambda_{22}\frac{d}{dt}\right)\partial_z w_2, \tag{27c}$$

which hold for $(x, z, t) \in \Omega_2$ as well as

$$(\mu\partial_z u_1 - \tau_{2,12}^{(1)}) - (\tau_{2,22} - \tau_{2,11})\partial_x h_1 = 0, \tag{27d}$$

at $z = h_1$ and

$$\tau_{2,12}^{(1)} + (\tau_{2,22} - \tau_{2,11})\,\partial_x h_2 = 0, \tag{27e}$$

at $z = h_2$.

Our first observation is that integration the leading order momentum balance in the upper layer (26b) w.r.t. z and using the boundary condition (26j) gives

$$p_2 = \tau_{2,22} - \partial_{xx} h_1 - \partial_{xx} h + \phi'(h). \tag{28}$$

Combining this expression with the next order momentum balance (27a) we obtain

$$0 = \partial_x(\partial_{xx} h_1 + \partial_{xx} h - \phi'(h)) + \partial_x(\tau_{2,11} - \tau_{2,22}) + \partial_z \tau_{2,12}^{(1)}. \tag{29}$$

We set

$$\bar{\tau}_2 := \tau_{2,11} - \tau_{2,22}. \tag{30}$$

Then integration of equation (29) gives

$$0 = h\partial_x(\partial_{xx} h_1 + \partial_{xx} h - \phi'(h)) + \int_{h_1}^{h_2} \partial_x \bar{\tau}_2 dz + \tau_{2,12}^{(1)}|_{z=h_2} - \tau_{2,12}^{(1)}|_{z=h_1}. \tag{31}$$

If we use this expression together with the next order boundary conditions (27d–27e) and set

$$S := \frac{1}{4h} \int_{h_1}^{h_2} \bar{\tau}_2 dz, \tag{32}$$

we obtain

$$0 = h\partial_x(\partial_{xx} h_1 + \partial_{xx} h - \phi'(h)) + 4\partial_x(hS) - \mu \partial_z u_1|_{z=h_1}. \tag{33}$$

In the next step we derive an equation for S. We first note that because of (26b–26c) and (26g) $u_2 = u_2(x,t)$ does not depend on z. We combine (27b) and (27c) to

$$\left(1 + \lambda_{21}\frac{d}{dt}\right)\bar{\tau}_2 = 4\left(1 + \lambda_{22}\partial_t + \lambda_{22} u_2 \partial_x\right)\partial_x u_2. \tag{34}$$

Integration of the left hand side of this equation yields

$$\int_{h_1}^{h_2} \left(1 + \lambda_{21}\frac{d}{dt}\right)\bar{\tau}_2 dz \tag{35}$$

$$= \int_{h_1}^{h_2} \left(1 + \lambda_{21}\partial_t + \lambda_{21} u_2 \partial_x + \lambda_{21} w_2 \partial_z\right)\bar{\tau}_2 dz \tag{36}$$

$$= \int_{h_1}^{h_2} \left(1 + \lambda_{21}\partial_t + \lambda_{21} u_2 \partial_x + \lambda_{21}(-z\partial_x u_2 + \partial_t h_1 + \partial_x(u_2 h_1))\partial_z\right)\bar{\tau}_2 dz \tag{37}$$

$$= 4h(1 + \lambda_{21}\partial_t + \lambda_{21} u_2 \partial_x) S \tag{38}$$

Hence, we obtain the equation for S

$$(1 + \lambda_{21}\partial_t + \lambda_{21}u_2\partial_x)S = (1 + \lambda_{22}\partial_t + \lambda_{22}u_2\partial_x)\,\partial_x u_2. \tag{39}$$

The kinematic and impermeability conditions imply the equation for h

$$\partial_t h = -\partial_x(h\,u_2). \tag{40}$$

In the last step we consider the evolution of the lower fluid and the interface h_1. From (26a) and (26e) we first obtain

$$u_1 = \frac{1}{2\mu}\partial_x p_1 z^2 + c\,z, \tag{41}$$

which we use for the evolution equation for h_1

$$\partial_t h_1 = -\partial_x \int_0^{h_1} u_1 dz = -\partial_x \left(\frac{1}{6\mu}h_1^3\partial_x p_1 + \frac{1}{2}h_1^2 c\right). \tag{42}$$

and determine the constant c from equation

$$\frac{1}{2\mu}\partial_x p_1 h_1^2 + c\,h_1 = u_2 \tag{43}$$

and by using (26h). We finally obtain the closed system of equations for h_1, h, S and u_2.

$$\partial_t h = -\partial_x(h\,u_2), \tag{44a}$$

$$\partial_t h_1 = \frac{1}{12\mu}\partial_x\left(h_1^3\partial_x p_1\right) - \frac{1}{2}\partial_x\left(h_1 u_2\right), \tag{44b}$$

$$0 = -\frac{1}{2}h_1\partial_x p_1 - h\partial_x\, p_2 + 4\partial_x(hS) - \frac{\mu}{h_1}u_2, \tag{44c}$$

$$0 = (1 + \lambda_{21}\partial_t + \lambda_{21}u_2\partial_x)S - (1 + \lambda_{22}\partial_t + \lambda_{22}u_2\partial_x)\,\partial_x u_2. \tag{44d}$$

where

$$p_1 = -(\sigma+1)\partial_{xx}h_1 - \partial_{xx}h, \quad \text{and} \quad p_2 = -\partial_{xx}h_1 - \partial_{xx}h + \phi'(h). \tag{45}$$

4 Newtonian liquid layers with large viscosity ratios

For the special case when $\lambda_{21} = \lambda_{22} = 0$ the upper liquid layer is a purely viscous fluid and we obtain the thin-film model

$$\partial_t h = -\partial_x(h\,u_2), \tag{46a}$$

$$\partial_t h_1 = \frac{1}{12\mu}\partial_x\left(h_1^3\partial_x p_1\right) - \frac{1}{2}\partial_x\left(h_1 u_2\right), \tag{46b}$$

$$0 = -\frac{1}{2}h_1\partial_x p_1 - h\partial_x\left(p_2 + \phi'(h)\right) + 4\partial_x(h\partial_x u_2) - \frac{\mu}{h_1}u_2. \tag{46c}$$

Interestingly, also the thin-film model (46) has not been considered before. Thin-film two-layer models that have been investigated in the literature, such as in [1, 35] or more recently in [23], considered only the case when the viscosity ratios μ_1/μ_2 of the two liquids are of $O(1)$.

This model ist also instructive as it will be used to derive an expression for an apparent slip, and compare to the dynamics of single layer dewetting films from a solid substrate. Moreover, it serves to contrast the behaviour of dewetting viscoelastic films, which we investigate in the last section.

4.1 Transitions in flow regimes

We investigate first the morphologies and dynamics of dewetting rims as they occur after the top layer ruptures. In particular, we contrast the results for the thin-film model for which $\mu_1/\mu_2 = O(1)$ with those for which $\mu_1/\mu_2 = O(\varepsilon^2)$, that we have derived in the previous section.

For moderate viscosity ratios, the resulting model has been derived previously derived in [1, 35] or in [23]. When we set the slip parameters in (3.5) in [23] to zero we obtain the system

$$\partial_t \mathbf{h} = \partial_x \left(Q \cdot \partial_x \mathbf{p} \right), \tag{47a}$$

where $\mathbf{h}$ denotes the vector $(h_1(x,t), h(x,t))$, $\mathbf{p} = (p_1(x,t), p_2(x,t))$, and the mobility matrix Q is given by

$$Q = \frac{1}{\mu} \begin{bmatrix} \dfrac{h_1^3}{3} & \dfrac{h_1^2 h}{2} \\ \dfrac{h_1^2 h}{2} & \dfrac{\mu}{3} h^3 + h_1 h^2 \end{bmatrix}, \tag{47b}$$

with

$$\begin{aligned} \partial_x p_1 &= -\partial_x \left((\sigma + 1) \partial_{xx} h_1 + \partial_{xx} h \right), \\ \partial_x p_2 &= -\partial_x \left(\partial_{xx} h + \partial_{xx} h_1 - \phi'(h) \right). \end{aligned}$$

From an asymptotic point of view, the two models correspond to two distinguished limits, and we expect an overlapping region of validity of (47) for small viscosity ratios μ_1/μ_2 with (46) for large μ. We present numerical results for each of the two models and different values for the viscosity ratios μ_1/μ_2 and μ, with a fixed choice for the remaining parameter $\sigma = 1$. Specifically, we set $\mu_1/\mu_2 = 0.001, 1, 1000$ in (47) and $\mu = 0.001, 1, 1000$ in (46).

We observe in fig. 2 that by changing the viscosity ratio in (47) the profile of the upper layer assumes for all values of μ_1/μ_2 shows a rim with an oscillatory decay towards the undisturbed parts of the upper layer. The wavelength of the oscillation increases as the ratio μ_1/μ_2 decreases. At the same time the profile of the liquid-liquid interface h_1 changes from almost no deviation from its equilibrium shape to a symmetric, to an unsymmetric profile, fig. 2 (bottom), with a more pronounced elevation near the dewetting front.

This tendency, of the unsymmetric shape of the h_1 interface is dramatically increased even for the thin-film model (46), even for the largest viscosity ratio both the rim of the upper layer and

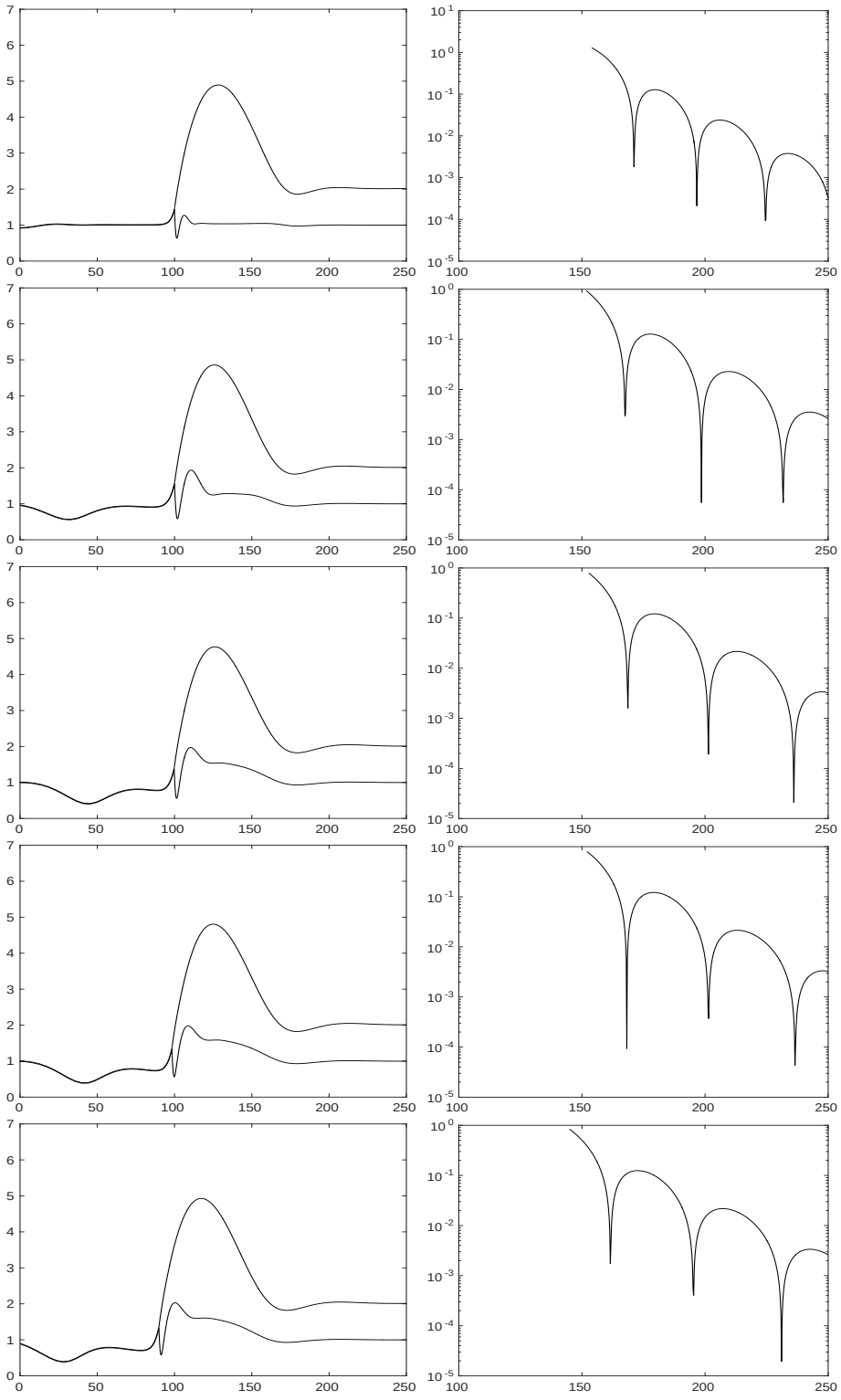

Figure 2: The moderate viscosity ratio model (47), with $\mu_1/\mu_2 = 10,\ 1,\ 0.1,\ 0.01,\ 0.001,$ from top to bottom.

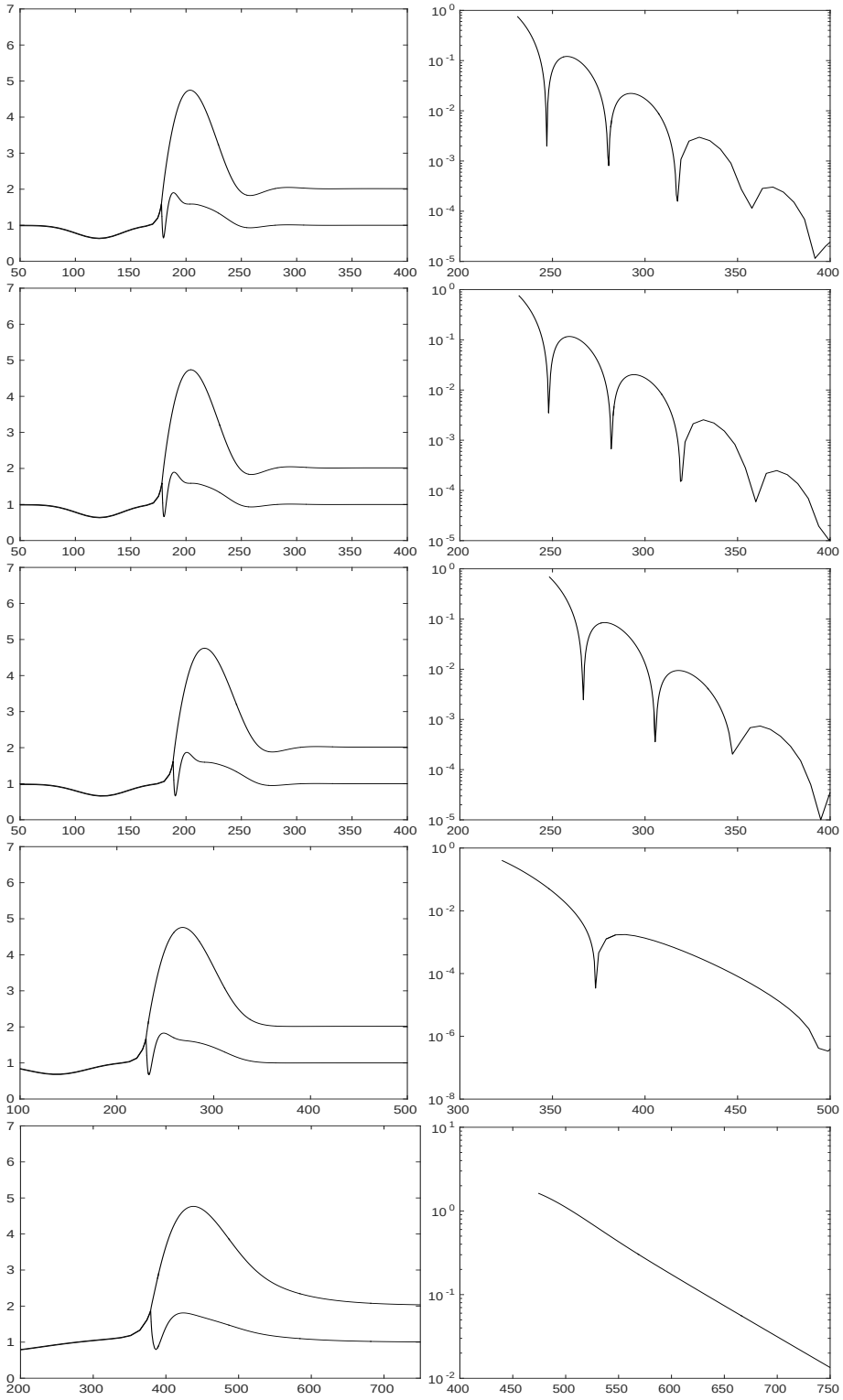

Figure 3: The small viscosity ratio model (46), with $\mu = 10,\ 1,\ 0.1,\ 0.01,\ 0.001$, from top to bottom.

the profile of the liquid-liquid interface have very pronounced asymmetric shapes. Moreover, as the value of the viscosity ratio is decreased in (46) the decay of the rims toward the undisturbed regions changes from oscillatory to a monotone behaviour as shown in fig. 3.

This characteristic change in profile has also been observed in the context of dewetting films from solid substrates that exhibit large slip [15, 33], where ist was shown that, while keeping other parameters fixed, the slip length controls this morphological transition. In the next section we will explore the connection between the viscosity ratios in a two layer system and the apparent slip.

4.2 Connection to apparent slip

The situation we study here with two layers of very different thickness and viscosity indeed arises for polymer solutions due to the depletion of the polymer fraction near the wall [9], where it has been seen as a source for apparent slip. For reviews on sources of apparent slip from experimental and theoretical perspective we also refer to [13, 19, 34, 39, 42], where it is contrasted with the so-called effective slip, where the molecules adjacent to the wall are thought to move, possibly facilitated by the presence of surface roughness, while in the depletion scenario, slippage is due to the lubrication effect of the reduced viscosity in the depletion layer near the wall. Mechanisms for the molecular segregation have been investigated in [40] and [11, 12], alongside with estimates for the depletion length.

We also note that bi-viscosity models have also been introduced to explain the occurrence of slip between to strongly segregated homopolymers. These separate into two nearly pure bulk layers, so that mixing only occurs in a thin interfacial layer, where the viscosity is reduced to the repulsion between the inter-penetrating chains [18].

For polymer melts, the theory for the origin of slip is quite different and relates the slip length b to the length of the polymer chains N and the entanglement length N_e via $b = aN^3/N_e^2$, where a is a polymer specific molecular size. The proximity of the surface is thought to increase the effective entanglement length, so that a gradient in the material properties does arise but is not fundamental for the appearance of slip. On the other hand, the magnitude of slip can be greatly modified by grafting different polymer chains to the substrate [2, 15, 16, 18] This is somewhat reminiscent of the mixing between the two polymer liquids in [18] and one may speculate if a similar mechanism as there may lead to a difference in the effective viscosity near to and further away from the that could contribute to the overall slip experienced by the bulk liquid as in the bi-viscosity situation modelled here.

To establish the connection to apparent slip we will focus here on very thin liquid substrates. To investigate this regime we introduce the quantity $b_1 := h_1/\mu$ and assume that

$$b_1 = O(1) \quad \text{and} \quad h_1,\, \mu \ll 1. \tag{48}$$

In this case we obtain from (46) the leading order equations

$$\partial_t h_2 = -\partial_x(h_2\, u_2), \tag{49a}$$

$$0 = h_2\partial_x(\partial_{xx}h_2 - V(h_2)) + 4\partial_x(h_2\partial_x u_2) - \frac{u_2}{b_1}. \tag{49b}$$

These two equations for h and u_2 are similar to the strong-slip lubrication model for the evolution of a single thin film on a solid substrate, where b_1 corresponds to the slip length. But in our case the quantity b_1 is not a constant. In fact it fulfils the transport equation

$$\partial_t b_1 = -\partial_x(b_1\, u_2). \tag{49c}$$

On the other hand, if we assume that $\sigma = \sigma^*/\mu^2$, with $\sigma^* = O(1)$, we obtain the system

$$\partial_t h_2 = -\partial_x(h_2\, u_2), \tag{50a}$$

$$0 = \frac{\sigma^*}{2} b_1 \partial_{xxx} b_1 + h_2 \partial_x(\partial_{xx} h_2 - V(h_2)) + 4\partial_x(h_2 \partial_x u_2) - \frac{u_2}{b_1}, \tag{50b}$$

$$\partial_t b_1 = -\frac{\sigma^*}{12} \partial_x(b_1^3 \partial_{xxx} b_1) - \partial_x(b_1\, u_2). \tag{50c}$$

For σ^* very large the last equation implies that $b_1 = B_1$ with a constant B_1. Hence,

$$\partial_t h_2 = -\partial_x(h_2\, u_2), \tag{51a}$$

$$0 = h_2 \partial_x(\partial_{xx} h_2 - V(h_2)) + 4\partial_x(h_2 \partial_x u_2) - \frac{u_2}{B_1}. \tag{51b}$$

Carrying this out for the moderate viscosity ratio model (47), with $m = \mu_1/\mu_2$, and the rescaling $h_1 = m b_1$, we obtain, for $m \ll 1$, $b_1 = O(1)$, that

$$\partial_t h_2 = -\partial_x \left[\left(\frac{1}{3} h^3 + b_1 h^2 \right) \partial_x \left(\partial_{xx} h_2 - V(h_2) \right) \right], \tag{52a}$$

$$\partial_t b_1 = -\partial_x \left[\frac{b_1^2 h_2}{2} \partial_x \left(\partial_{xx} h_2 - V(h_2) \right) \right]. \tag{52b}$$

Again, b_1 plays the role of an effective slip for the evolution of the top, i.e. liquid-air interface.

If we assume strong surface tension by also letting $\sigma = \sigma^*/m^2$, with $\sigma^* = O(1)$, we obtain in the limit $m \to 0$,

$$\partial_t h_2 = -\partial_x \left[\sigma^* \frac{b_1^2 h_2}{2} \partial_{xxx} b_1 + \left(\frac{1}{3} h^3 + b_1 h^2 \right) \left(\partial_{xx} h_2 - V(h_2) \right) \right] \tag{53a}$$

$$\partial_t b_1 = -\partial_x \left[\sigma^* \frac{b_1^3}{3} \partial_{xxx} b_1 + \frac{b_1^2 h_2}{2} \partial_x \left(\partial_{xx} h_2 - V(h_2) \right) \right]. \tag{53b}$$

If, in fact, σ^* is large, this reduces to $b_1 = B_1$ with a constant B_1, and

$$\partial_t h_2 = \left[\left(\frac{1}{3} h^3 + \frac{1}{4} B_1 h^2 \right) \partial_x \left(\partial_{xx} h_2 - V(h_2) \right) \right]. \tag{54}$$

Quantitative accuracy of our estimate of the effective slip can be obtained in particular for the large μ case, by verifying that for a given far-field value of $b_1 = h_1/\mu$ the transition from an oscillatory to a monotonic profile h_2 or vice-versa occurs for (46) and (49) under identical conditions. In fig. 4 we have choosen h_1 and μ such that b_1 is in the order of magnitude of β compared to the results in [33]. We obtain a transition from oscillatory to monotonic profiles for the top layer in the numerical solutions of (46), similarly to the results in [33] (fig. 8) for the strong-slip model with the corresponding $\beta = b_1$.

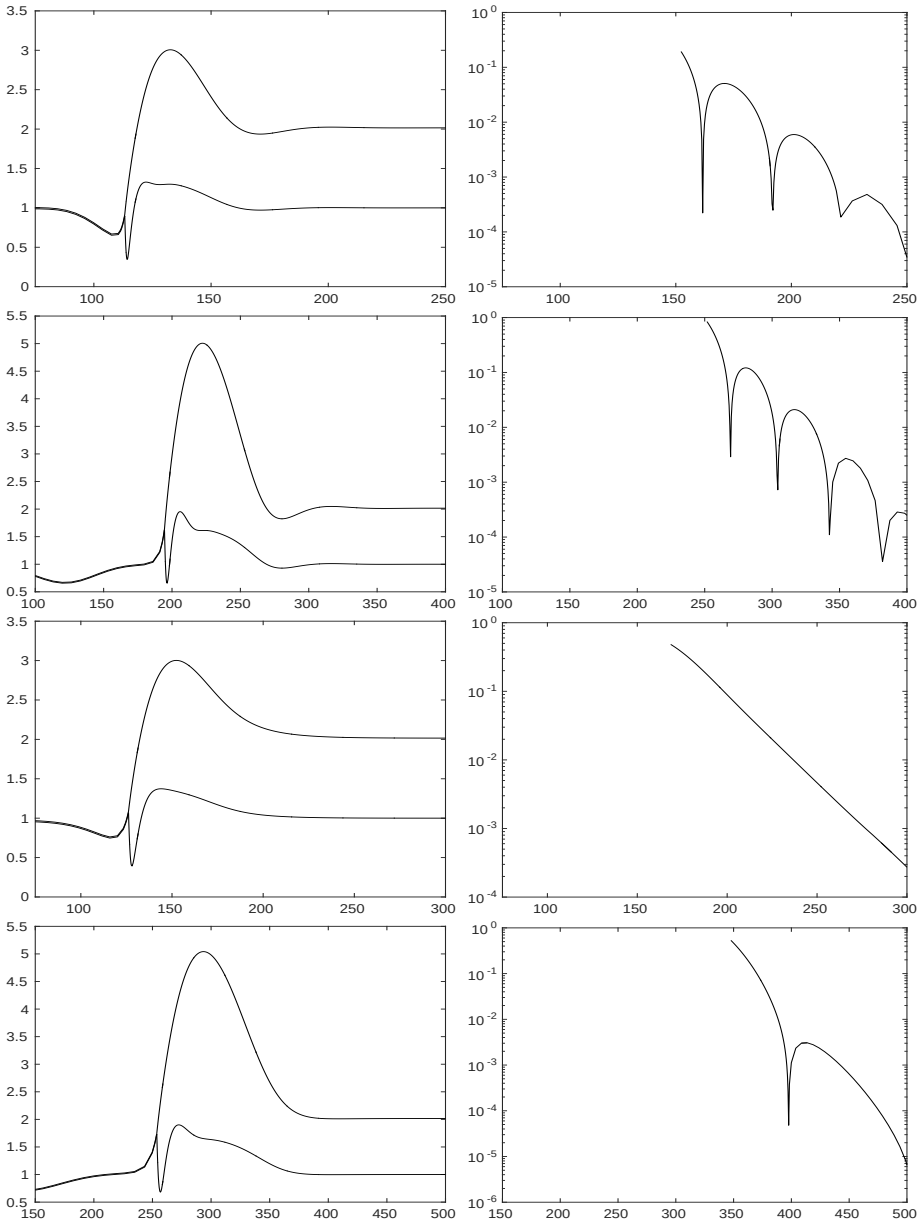

Figure 4: The small viscosity ratio model (46), top row : $\mu = 1$, morphology (left) and semilogy (right), early stage; 2nd row: top row : $\mu = 1$, morphology (left) and semilogy (right), later stage; 3rd row : $\mu = 0.01$, morphology (left) and semilogy (right), early stage; bottom row: top row : $\mu = 0.01$, morphology (left) and semilogy (right), later stage.

5 Dewetting viscoelastic films: dynamics and morphology

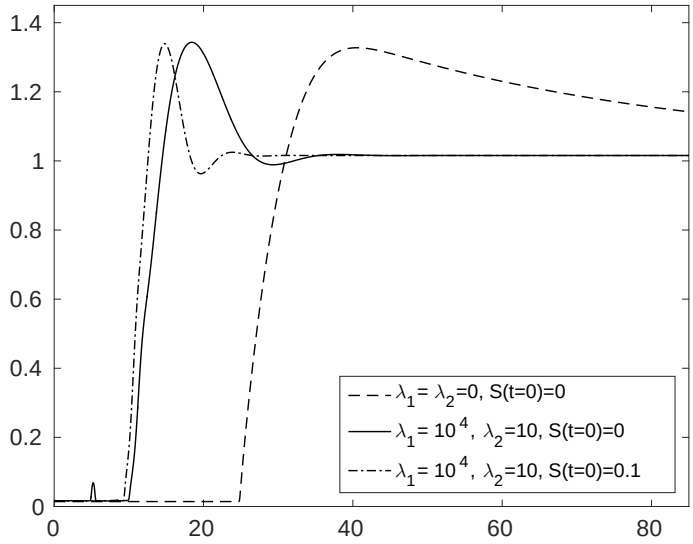

Figure 5: The strong-slip, viscoelastic model on a solid substrate (55), comparison of the morphologies for different values of λ_1, λ_2 and initial conditions for S.

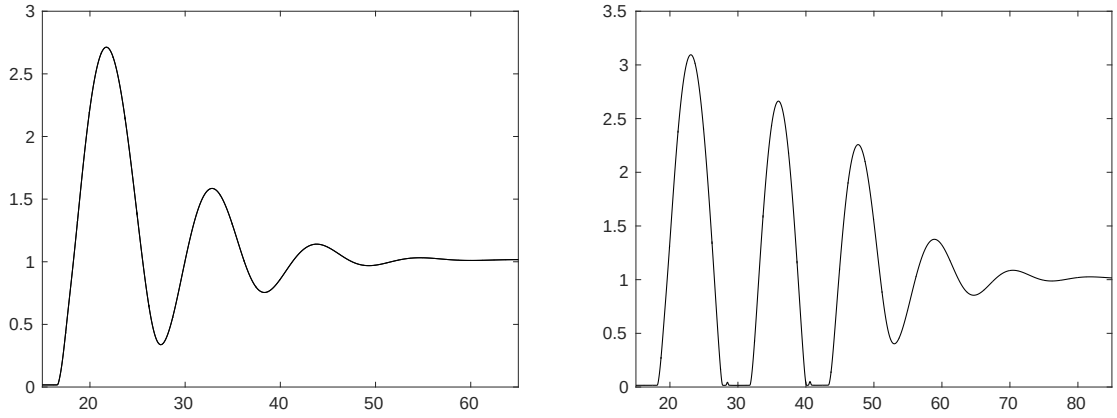

Figure 6: The strong-slip, viscoelastic model on a solid substrate (55), morphologies for large λ_1 at two different times.

We now return to the dewetting thin film problem with a corotational Jeffreys' model. There are a number of theoretical and experimental studies concerning the morphologies and dewetting rates of single layer viscoelastic dewetting films [3, 5, 22], in particular the period after rupture and in stressed state, for example due to prior spin coating process [38, 41, 44] . Our models enable to simulate the fully nonlinear viscoelastic behaviour for different parameter choices. Here we give a few illustrations for large values of λ_{21} and inparticular compare dynamics and morphologies to the Newtonian model.

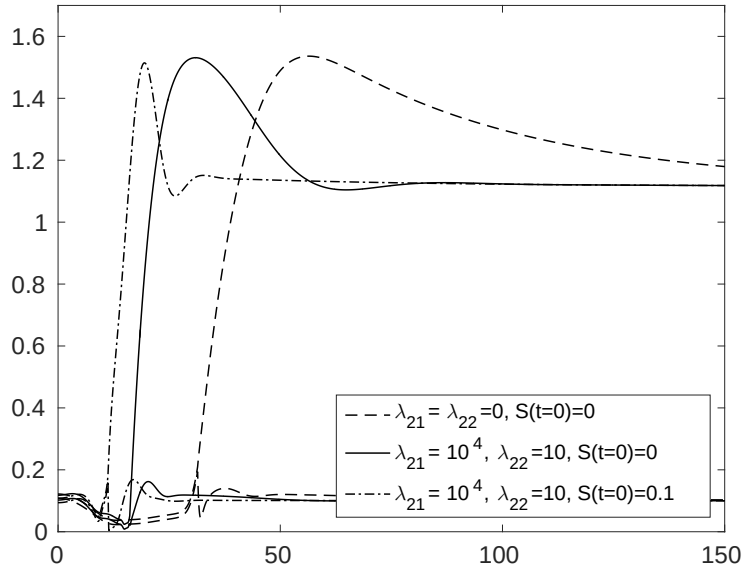

Figure 7: The small viscosity ratio, viscoelastic model (44), comparison of the morphologies for different values of λ_1, λ_2 and initial conditions for S.

In the previous section we showed a strong connection of the small viscosity ratio model (46) to the strong-slip model on a solid substrate. Obviously, a similar derivation be can be carried out in the viscoelastic case. In fact, considering the same limit in (44) one ends up with

$$\partial_t h_2 = -\partial_x(h_2\, u_2), \tag{55a}$$

$$0 = h_2\partial_x(\partial_{xx}h_2 - \phi'(h_2)) + 4\partial_x(h_2\partial_x u_2) - \frac{u_2}{B_1}, \tag{55b}$$

$$0 = (1 + \lambda_1\partial_t + \lambda_1 u_2\partial_x)S - (1 + \lambda_2\partial_t + \lambda_2 u_2\partial_x)\,\partial_x u_2. \tag{55c}$$

The latter model can be found for example in [5].

In order to distinguish the impact of the viscoelastic rheology from the influence of a deformable liquid substrate on the morphology of a dewetting film after rupture, it is instructive to first consider the case of the viscoelastic film dewetting from a solid substrate. The latter case is also interesting since its rupture and subsequent dewetting dynamics has not been investigated before within a thin-film framework.

As a first example we compare in fig. 5 an early stage of the dynamics given by (55) for $B_1 = 600$. In the case $\lambda_1 = \lambda_2 = 0$ we observe the expected asymmetric shape of the rim, where the maximum of the rim is connected to the the undisturbed film by an almost straight line. This behaviour changes if one includes viscoelastic effects. To illustrate this we have choosen $\lambda_1 = 10000$ and $\lambda_2 = 10$. We can make several interesting observations. First, the shape of the rim attains the form of a parabola similar to the one obtained in the weak -slippage case. Another immediate observation is that the dewetting rate of the contact line is significantly slower in the viscoelastic case. Finally, we see that the first two effects are enhanced when the initial value of the quantity S is nono-zero, which means that we impose a non-zero initial stress. Here we have chosen the value $S(t = 0, x) \equiv 0.1$.

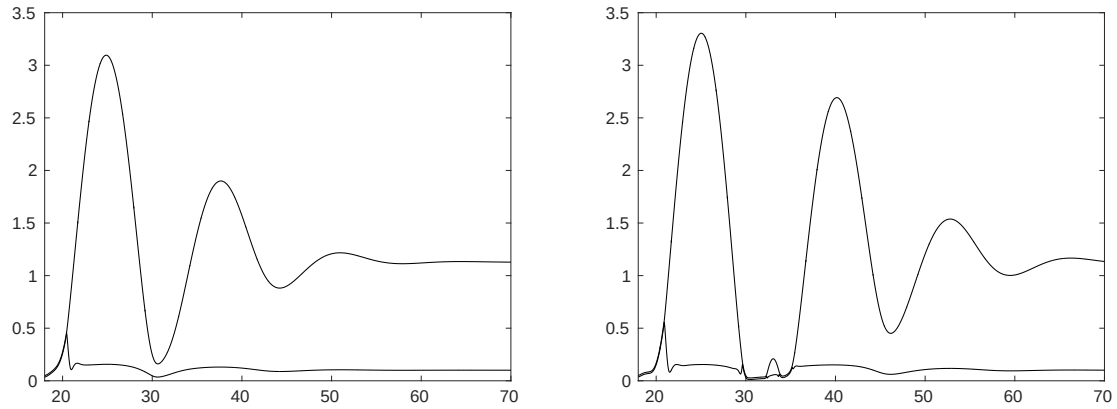

Figure 8: The small viscosity ratio, viscoelastic model (44), morphologies for large λ_1 at two different times.

In fig. 6 the evolution of the case with non-zero initial S is shown. We observe that while the dewetting rim grows, it quickly pinches off, forming a new constactline. Hence, instead of a retracting film we observe that a series of droplets is formed. Moreover, for certain parameter settings, also smaller secondary droplets pinch off just before the new contact line forms and is aresult of a non-zero initial stress. In the case of $S(t = 0, x) \equiv 0$ the rim retracts while remaining stable.

Next, we consider the corresponding situation for the bi-layer model, i.e. we consider (44) with a very low viscosity ratio and a small initial thickness of the liquid substrate; here we chose $\mu = 1/6000$ and $h_1(t = 0, x) \equiv 0.1$. In fig. 7 we observe almost the same behaviour as in fig. 5. In the Newtonian case, the asymmetric rim shape is obtained, while in the two viscoelastic cases the rim attains a more parabolic shape. Also here we encounter that the contact line moves much slower in the presence of viscolelastic effects. In fig. 8 we again observe that for $S(t = 0, x) \equiv 0.1$ there is an immediate formation of droplets. However, there are some differences in the size of the droplets compared to the case of an solid substrate. In particaler, the smaller secondary droplets are larger than in 6.

While these examples can only provide a first glimpse into the rich dynamic and morphological structure of the evolving viscoelastic films, a systematic parameter study is the topic of an upcoming investigation.

6 Conclusion

In this work we derived conditions that allow an asymptotcally consistent reduction of governing free boundary problem for a two-layer liquid system to a thin-film model with fully nonlinear viscoelastic rheology, such as the corotational Jeffreys' model. These conditions show that this is controlled by the order of magnitude of the viscosity ratio of the liquid bi-layer.

We also revisited the Newtonian case and showed that in this case the corresponding thin-film model reduces to model similar in structure to the so-called strong-slip model for the one layer

situation. In particular, also here, the well-known transition [15] from oscillatory to monotone decay of the rim tail for increasing slip lengths can also be observed for the bi-layer, here for decresing viscosity ratio. Similarly, as done in [33] one can capture this transition using a linear stability analysis about the undisturbed upper layer.

In summary, when linearising (46), using the ansatz

$$h_1 = a + \exp(\alpha\zeta), \quad h = 1 + \chi \exp(\alpha\zeta), \quad \zeta = x - s(t),$$

two equations for χ, can be obtained and σ for given $\dot{s}(t)$. A non-trivial solution for χ only exists if the coefficient matrix vanishes. This gives a high-order (up to 8th order) polynomial equation for σ.

$$\dot{s} - \dot{s}\frac{a}{2}\chi = \frac{a^3}{12\mu}\left((\sigma+1)\alpha^3 + \chi\alpha^3\right), \tag{56}$$

$$0 = \frac{a^2}{2}\left((\sigma+1)\alpha^3 + \chi\alpha^3\right) + a\left(\alpha^3 + \chi\alpha^3 - \phi\chi\alpha\right) + 4a\dot{s}\chi\alpha^2 - \mu\dot{s}\chi. \tag{57}$$

which then can be solved σ, where only the roots which have Re $\sigma < 0$ are relevant so that $\exp(\sigma\xi)$ decays as $\chi \to \infty$. One can then derermine how many roots qualify under this criterion and which of them have non-zero imaginary part or change their imaginary part from zero to non-zero for varying $\dot{s}$.

We then exploited this fact to show that for the limiting case of a liquid substrate, that is thin compared to the dewetting film on top, an expression for an apparent slip can be derived.

Our numerical simulations on dewetting viscoelastic films shortly after the rupture process and using stressed initial conditions showed that, by varying the time relaxation parameters λ_{21} and λ_{22} rather surprising new morphologies can be obtained. They reveal that in the limiting Newtonian case the ri shows a particular asymmetric shape as has been shown for dewetting liquid films with large slip for the single layer case. In contrast for increasing λ_{12} these asymmetric morphology is relaxed but other new structures emerge. This is also accompanied by varying dewetting regimes. An intriguing morphology for large λ_{12} shows pinch off of the tail of the rim and a structure reminiscient to the “beads on a string” structure observed before in viscoelastic (Oldroyd-B) strings, see for example [29, 31]. These and further regimes will be investigated systematically in an upcoming work.

Acknowledgements

SJ gratefully acknowledges the support by the DFG of the project “Structure formation in thin Bi-layers” within the priority programme SPP 1506 “Transport at Fluidic Interfaces”. The authors would also like to thank Tobias Ahnert for fruitful discussions on the numerics.

References

[1] D. Bandyopadhyay, R. Gulabani, and A. Sharma. Instability and dynamics of thin liquid bilayers. *Ind. Eng. Chem. Res*, 44(5):1259–1272, 2005.

[2] O. Bäumchen, R. Fetzer, and K. Jacobs. Reduced interfacial entanglement density affects the boundary conditions of polymer flow. *Phys. Rev. Lett.*, 103:247801, 2009.

[3] O. Bäumchen and K. Jacobs. Slip effects in polymer thin films. *Journal of Physics: Condensed Matter*, 22(3):033102, 2010.

[4] K. Binder and H. L. Frisch. Interfacial profile between coexisting phases of a polymer mixture. *Macromolecules*, 17(12):2928–2930, 1984.

[5] R. Blossey. Viscoelastic thin films. In *Thin Liquid Films*, Theoretical and Mathematical Physics, pages 89–115. Springer Netherlands, 2012.

[6] R. Blossey, A. Münch, M. Rauscher, and B. Wagner. Slip vs. viscoelasticity in dewetting thin films. *Eur. Phys. J. E - Soft Matter*, 20:267–271, 2006.

[7] F. Brochard-Wyart, G. Debregeas, R. Fondecave, and P. Martin. Dewetting of supported viscoelastic polymer films: Birth of rims. *Macromolecules*, 30:1211–1213, 1997.

[8] F. Brochard-Wyart, P. Martin, and C. Redon. Liquid/liquid dewetting. *Langmuir*, 9(12):3682–3690, 1993.

[9] J. Cayer-Barrioz, D. Mazuyer, A. Tonck, and E. Yamaguchi. Drainage of a Wetting Liquid: Effective Slippage or Polymer Depletion? *Tribology Letters*, 32(2):81–90, 2008.

[10] R. V. Craster and O. K. Matar. On the dynamics of liquid lenses. *J. Colloid and Interface Sci.*, 303:503–506, 2006.

[11] P. G. de Gennes. Polymer solutions near an interface. 1. adsorption and depletion layers. *Macromolecules*, 14:1637–1644, 1981.

[12] P. G. de Gennes. Polymers at an interface: a simplified view. *Advances in Colloid and Interface Science*, 27(3):189–209, 1987.

[13] B. V. Derjaguin and N. V. Churaev. Structure of water in thin layers. *Langmuir*, 3:607–612, 1987.

[14] A. D. F. Dunbar, P. Mokarian-Tabari, A. J. Parnell, S. J. Martin, M. W. A. Skoda, and R. A. L. Jones. A solution concentration dependent transition from self-stratification to lateral phase separation in spin-cast PS:d-PMMA thin films. *Eur. Phys. J. E - Soft Matter*, 31:369–375, 2010.

[15] R. Fetzer, K. Jacobs, A. Münch, B. Wagner, and T. P. Witelski. New slip regimes and the shape of dewetting thin liquid films. *Phys. Rev. Lett.*, 95:127801, 2005.

[16] R. Fetzer, A. Münch, B. Wagner, M. Rauscher, and K. Jacobs. Quantifying Hydrodynamic Slip: A Comprehensive Analysis of Dewetting Profiles. *Langmuir*, 23(21):10559–10566, 2007.

[17] L. S. Fisher and A. A. Golovin. Instability of a two-layer thin liquid film with surfactants: Dewetting waves. *J. Colloid and Interface Sci.*, 307(1):203–214, 2007.

[18] J. L Goveas and G. H Fredrickson. Apparent slip at a polymer-polymer interface. *Eur. Phys. J. B - Condensed Matter and Complex Systems*, 2(1):79–92, 1998.

[19] S. Granick, Y. Zhu, and H. Lee. Slippery questions about complex fluids flowing past solids. *Nature Materials*, 2:221–227, 2003.

[20] S. Y. Heriot and A. L. Jones. An interfacial instability in a transient wetting layer leads to lateral phase separation in thin spin-cast polymer-blend films. *Nature Materials*, 4:782–786, 2005.

[21] S. Herminghaus, K. Jacobs, and R. Seemann. Viscoelastic dynamics of polymer thin films and surfaces. *Eur. Phys. J. E*, 12(1):101–110, 2003.

[22] S. Herminghaus, R. Seemann, and K. Jacobs. Generic morphologies of viscoelastic dewetting fronts. *Phys. Rev. Lett.*, 89(5):056101, 2002.

[23] S. Jachalski, D. Peschka, A. Münch, and B. Wagner. Impact of interfacial slip on the stability of liquid two-layer polymer films. *J. Engr. Math.*, 86(1):9–29, 2014.

[24] J.-F. Joanny. Wetting of a liquid substrate. *Physicochemical Hydrodynamics*, 9(1-2):183–196, 1987.

[25] M. B. Jones, D. L. S. McElwain, G. R. Fulford, M. J. Collins, and A. P. Roberts. The effect of the lipid layer on tear film behaviour. Bull. Math. Biol., 68:1355–1381, 2006.

[26] R. E. Khayat. Transient two-dimensional coating flow of a viscoelastic fluid film on a substrate of arbitrary shape. *J. Non-Newton. Fluid Mech.*, 95(2–3):199–233, 2000.

[27] P. E. King-Smith, B. A. Fink, J. J. Nichols, K. K. Nichols, R. J. Braun, and G. B. McFadden. The contribution of lipid layer movement to tear film thinning and breakup. *IOVS*, 50:2747–2756, 2009.

[28] J. J. Kriegsmann and M. J. Miksis. Steady motion of a drop along a liquid interface. *SIAM Journal of Applied Mathematics*, 64(1):18–40, 2003.

[29] J. Li and M. A. Fontelos. Drop dynamics on the beads-on-string structure for viscoelastic jets: A numerical study. *Physics of Fluids*, 15(4):922–937, 2003.

[30] G. M. Homsy M. A. Spaid. Stability of newtonian and viscoelastic dynamic contact lines. *Physics of Fluids*, 8(2):460–478, 1996.

[31] G. H. McKinley. Visco-elasto-capillary thinning and break-up of complex fluids. *Submitted to Annual Rheology Reviews*, 2005.

[32] A. Münch, B. Wagner, M. Rauscher, and R. Blossey. A thin-film model for corotational jeffreys fluids under strong slip. *Eur. Phys. J. E*, 20(4):365–368, 2006.

[33] A. Münch, B. Wagner, and T. P. Witelski. Lubrication models with small to large slip lengths. *J. Engr. Math.*, 53:359–383, 2006.

[34] C. Neto, D. R. Evans, E. Bonaccurso, H.-J. Butt, and V. S. J. Craig. Boundary slip in newtonian liquids: a review of experimental studies. *Rep. Prog. Phys.*, 68:2859–2897, 2005.

[35] A. Pototsky, M. Bestehorn, D. Merkt, and U. Thiele. Morphology changes in the evolution of liquid two-layer films. *The Journal of chemical physics*, 122:224711, 2005.

[36] O. Hassager R. B. Bird, R. C. Armstrong. *Dynamics of Polymeric Fluids (Vol. 1)*. Wiley & Sons, New York, 1977.

[37] M. Rauscher, A. Münch, B. Wagner, and R. Blossey. A thin-film equation for viscoelastic liquids of jeffreys type. *Eur. Phys. J. E*, 17(3):373–379, 2005.

[38] G. Reiter, M. Sferrazza, and P. Damman. Dewetting of thin polymer films at temperatures close to the glass transition. *Eur. Phys. J. E*, 12(1):133–138, 2003.

[39] J. Sanchez-Reyes and L. A. Archer. Interfacial slip violations in polymer solutions: role of microscale surface roughness. *Langmuir*, 19:3304–3312, 2003.

[40] R. Tuinier and T. Taniguchi. Polymer depletion-induced near an interface. *J. Phys. Condens. Matter*, 17:L4–L9, 2005.

[41] T. Vilmin and E. Raphael. Dewetting of thin viscoelastic polymer films on slippery substrates. *Europhysics Letters*, 72:781, 2005.

[42] O. I. Vinogradova. Slippage of water over hydrophobic surfaces. *Int. J. Miner. Process*, 56:31–60, 1999.

[43] Y. L. Zhang, O. K. Matar, and R. V. Craster. Surfactant spreading on a thin weakly viscoelastic film. *J. Non-Newton. Fluid Mech.*, 105(1):53–78, 2002.

[44] F. Ziebert and E. Raphaël. Dewetting of thin polymer films: Influence of interface evolution. *Europhysics Letters*, 86(4):46001, 2009.